Evaluating possible spectroscopic variation of Bennu's sampling site

A. Praet, G. Poggiali, M. A. Barucci, B. E. Clark, X. -D. Zou, A. A. Simon, H. H. Kaplan, J. -Y. Li, C. Alcaria

Monthly Notices of the ROYAL ASTRONOMICAL SOCIETY

MNRAS **519,** 1464–1475 (2023) https://doi.org/10.1093/mnras/stac2969
Advance Access publication 2022 October 19

Evaluating possible spectroscopic variation of Bennu's sampling site

A. Praet [1], G. Poggiali [1]★, M. A. Barucci [1], B. E. Clark,[2] X.-D. Zou,[3] A. A. Simon [4], H. H. Kaplan,[4] J.-Y. Li[3] and C. Alcaria[1]

[1]*LESIA-Observatoire de Paris, Université PSL, CNRS, Université Paris Cité, Sorbonne Université, 5 place Jules Janssen, F-92190 Meudon, France*
[2]*Department of Physics and Astronomy, Ithaca College, Ithaca 14850, NY, USA*
[3]*Planetary Science Institute, Tucson, AZ 85719, USA*
[4]*NASA Goddard Space Flight Center, Greenbelt, MD 20771, USA*

Accepted 2022 October 11. Received 2022 October 10; in original form 2022 September 8

ABSTRACT

The OSIRIS-REx spacecraft completed the first part of the primary objective by successfully sampling the surface of asteroid (101955) Bennu and storing the acquired sample in the re-entry capsule. The sampling 'Touch-And-Go' (TAG) maneuver was performed nominally at the primary sampling site, Nightingale, in Bennu's Northern hemisphere. As a consequence of the TAG, material at the sampling site was mobilized and the morphology of the area was altered. This event offered a unique opportunity to investigate, in detail, the subsurface of asteroid Bennu giving access to fine grained and less altered material from Nightingale crater. We performed a detailed study on the infrared spectrum in the Nightingale region to search for modification resulting from the sampling event by analysing different features: slope, the H_2O–OH^- related absorption band in the 2.7 μm region, and other possible features. Our results show that, despite visible alteration of the TAG location detected by cameras, no strong variations are observed in the near-infrared bands and their quantitative evaluation is not possible beyond all the instrumental effects, although some changes may have occurred. We confirm that the infrared spectrum of the sampling site becomes redder with respect to the pre-TAG observations, conceivably due to fine material mobilization and exposure of less altered material, as confirmed by decreased spectral convexity. We identify possible modification of hydrated band at 2.7 μm but with some concerns due to data quality. However, our results place new constraints on the nature of Bennu's subsurface material and the sample collected by OSIRIS-REx.

Key words: solid state: volatile – space vehicles – techniques: spectroscopic – minor planets, asteroids: individual: Bennu, OSIRIS-REx – planets and satellites: surfaces.

1 INTRODUCTION

The OSIRIS-REx spacecraft (Lauretta et al. 2017) successfully performed a sample collection maneuver on the surface of primitive dark asteroid (101955) Bennu on 2020 October 20th in order to accomplish the mission main objective and return a surface sample of the carbonaceous asteroid to Earth in 2023. The scientific payload intensively studied the asteroid surface before the Touch-And-Go (TAG) sampling event to characterize Bennu's surface and to select the best sampling site. In particular, the OSIRIS-REx Visible and InfraRed Spectrometer (OVIRS; Reuter et al. 2018) surveyed Bennu's surface in the wavelength range of 0.4 to 4.3 μm during the global mapping campaign. These intensive observations found a prominent 2.7 μm absorption feature that exists everywhere on the asteroid surface (minimum position at 2.74 ± 0.01 μm) associated with OH^- and H_2O bound in hydrated phyllosilicates (Hamilton et al. 2019; Simon et al. 2020a). The presence of Mg-rich phyllosilicates were confirmed by Simon et al. (2020b) who found minor absorption bands centered near 1.4, 1.8, and 2.3 μm linked with overtones and combinations of the OH^- stretching and H_2O bending vibrational mode. Other minor bands are suggested to be related to the presence of phyllosilicates, carbonates, organics, or other mineral species (Simon et al. 2020b). Recently, Praet et al. (2021a), using data from the Detailed Survey: Equatorial Station 3 (EQ3) phase, estimated the global average hydrogen content of the hydrated phyllosilicate H_2O and OH^- groups on Bennu's surface to be 0.71 ± 0.16 wt per cent. This result was evaluated using several spectral parameters: the Normalized Optical Path Length (NOPL); the Effective Single-Particle Absorption Thickness (ESPAT; Milliken & Mustard 2007); and Gaussian modelling of the phyllosilicate absorption feature. The value is consistent with the hydration range of aqueously altered carbonaceous chondrite (CC) meteorites such as CMs and the C2 Tagish Lake. Spatial variations in hydrogen content were found on Bennu, mostly linked to surface geomorphology partially inherited from its parent body. Notably, the mission primary sampling site, Nightingale, was found to have a slightly higher hydrogen content than average Bennu (Praet et al. 2021a).

Image data acquired by OSIRIS-REx showed that Bennu, a rubble pile asteroid, has a rough and rocky surface characterized by meter-scale boulders (Dellagiustina et al. 2019; Walsh et al. 2019; Jawin et al. 2020). Despite its rocky nature, the Nightingale site was selected for sample collection both for the relative absence of large boulders (and therefore safety during the collection maneuver) and

★ E-mail: giovanni.poggiali@obspm.fr

the relative abundance of fine material (particle size < 2cm). During the sample acquisition event on 2020 October 20th, the TAG Sample Acquisition Mechanism, TAGSAM (Bierhaus et al. 2018) collected a bulk sample from the Nightingale crater by releasing a jet of high-purity nitrogen gas, thus setting dust and particles into motion towards the collection chamber. As is visible in the images acquired during the manoeuvre, abundant material with small particle size was lofted and ejected by the gas release. Pictures collected in the phases following the gas release show a dark dust cloud accompanied by movement of larger debris. Dust deposition on the spacecraft exterior induced degradation and other effects in instrument optics, including dust detected on the OVIRS primary mirror, as observed by the Science Team during post-sampling checkout of the scientific payload (Lauretta et al. 2022).

Before departure towards the Earth on 2021 April 7th, the OSIRIS-REx spacecraft approached Bennu once more to perform global observations in order to document surface changes resulting from the TAG event, in particular, around the Nightingale area. These new data sets, acquired during the so-called Bennu Final Flyby (BFF), were obtained using the same observational sequence utilized during the global detailed survey campaign before sample collection. Before- and after-TAG observations of Bennu offer a unique opportunity to understand the properties of the asteroid surface and, by characterizing sub-surface newly-exposed material, to unveil the evolution and modification of Bennu's surface. The level of detail and the large amount of data available from OVIRS observations give us the possibility of an unprecedented level of investigation of an asteroid surface. The OSIRIS-REx data will provide scientists with data to work on for years, and our analysis inferring the H_2O/OH^- content in the subsurface may lead to new discoveries about the penetration of thermal waves on Bennu's surface and the overall alteration of asteroid rock surfaces. Moreover, joining our results with detailed analysis that will be performed on the returned sample in September 2023 will substantially improve our knowledge of asteroid stratigraphy and surface evolution.

In the following sections, we report on the methods and results of our analysis of OVIRS infrared data acquired before and after the TAG event, focusing on the Nightingale area. We compare measurements of the newly exposed surface with those obtained and analysed before TAG by Praet et al. (2021a).

2 METHODS

In this work, we analysed OVIRS spectra from the EQ3 and BFF phases of the OSIRIS-REx mission, specifically those that were collected, respectively, on 2019 May 9th (pre-TAG) and on 2021 April 7th (post-TAG). Spectra in these data sets cover the entire asteroid surface including the mission's primary sampling site, Nightingale, with different footprint resolutions: $\sim$ 20 m in EQ3 and $\sim$ 12 m in BFF. More details on orbital parameters and observational conditions for both of the data sets used in this work are described in the Appendix. OSIRIS-REx calibration pipeline include resampling and thermal tail removal as described in Simon, Reuter & Lauretta (2021). Both data sets were finally filtered for incidence and emission angles < 70° to avoid geometric artifacts (Zou et al. 2021). The final data sets result in 7089 spectra for the EQ3 station and 23381 spectra for the BFF. We performed two separate analyses of the sampling site spectra before and after the TAG event: in the first one, we focused on the single spectrum and its variability in regions nearby the Nightingale crater; in the second analysis, we evaluated and compared maps before and after the TAG event to study, in detail, possible variation in the near-infrared hydrated feature parameters (band minimum position, band depth, band area, and NOPL).

For the single spectrum analysis, following the method applied by Kitazato et al. (2021), we compared the spectra acquired in the Nightingale site with those from regions far from the sampling site. Areas were selected in EQ3 and BFF to be as comparable as possible in terms of position, although some differences in footprint dimension arise from the different altitudes of the observations. For each area, continuum removed spectra were evaluated fitting a second degree polynomial curve in the region of interest around the hydrated band at 2.7 μm, between 2 and 3.5 μm, similar to the method applied in Simon et al. (2020a). Moreover, the spectra were divided by the global average of Bennu's surface (obtained averaging all the spectra of the respective data set and presented in Appendix Fig. A1) to highlight possible differences between the Nightingale site and the rest of the surface, similar to what was done to extract the spectral properties of exogenous material (Dellagiustina et al. 2019). In the Appendix, we present an analysis on the effect of ratioing using a different average, showing there is no strong effect on the results (Fig. A3). Spectra in this analysis were not photometrically corrected since no direct comparisons are made between data from the two different observational stations, and observational conditions were similar (see Appendix Table A1 for more detail).

For the mapping analysis, in addition to the calibration pipeline, all data for EQ3 and BFF were photometrically corrected (Zou et al. 2021) using the McEwen model to the reference geometry of (0°, 30°, 30°) for incidence, emission, and phase angles, respectively. This allow us to compare data sets acquired with different geometries. The band minimum position was evaluated by fitting a seventh-order polynomial function between 2.69 and 2.85 μm and locating the inflection point of its first derivative, similarly to the technique described in Hamilton et al. (2019). Using the same method described in the previous work (Praet et al. 2021a), band depth and band area were evaluated using a linear continuum fitted between 2.6 and 3.3 μm. In addition, we evaluated the NOPL for each individual absolute reflectance spectrum analysed using the technique described in our previous work (Praet et al. 2021a,b). The NOPL and band depth parameters were calculated at the wavelength of the band minimum position (2.73 μm). Maps of different areas on Bennu's surface were created using the 200-k facet Palmer shape model (Barnouin et al. 2019). Weighted average values for each spectral parameter were evaluated on each facet using all the overlapping OVIRS spots and weighing the result with the percentage of overlap between the OVIRS spot and the facet (Ferrone et al. 2021). Final maps obtained for each parameter were ratioed between the two observational stations (BFF and EQ3) and superimposed on to Bennu's global basemap (Bennett et al. 2021).

Comparisons between BFF and other data sets acquired before the TAG event are conditioned by several caveats; proper assessment of this caveats are needed to obtain reliable results. Therefore, we present here a summary of our knowledge and quality tests on possible effects affecting our analysis. As observed by cameras on OSIRIS-REx, the TAG event produced a large mobilization of fine and coarse material from the Nightingale site. The debris and dust cloud surrounded the spacecraft during the sample acquisition causing a deposition of dust particles on instruments optics, degrading performance. The fraction of transmission for the OVIRS instrument was estimated to be 95 per cent of its original value after the TAG event, due to dust contamination (Lauretta et al. 2022). Presence of dust on the mirror affects all the measurements obtained during BFF observation. However, the dust on the mirror was constant during the observation and the ratioing procedure largely removed the

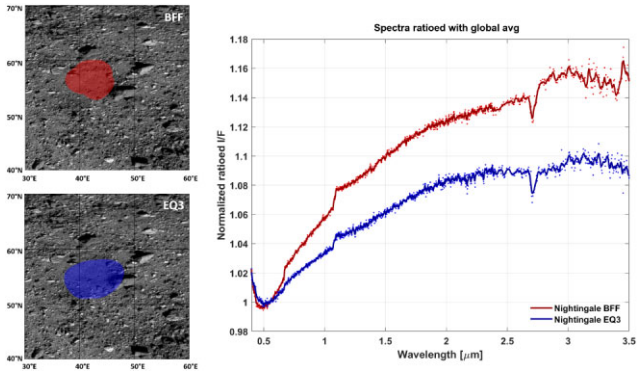

Figure 1. Right-hand panels: Spectra of Nightingale before (blue, average of two spectra) and after (red, average of three spectra) the sampling event ratioed to the global average of the data set from which the spectra were extracted (respectively, EQ3 and BFF). Dots show the original data and continuous lines show the smoothed spectra. Left-hand panels: The maps on the left show the positions of OVIRS footprints overlain on the Bennu global mosaic, colour coded with the spectra shown on the right. The spectrum of the sampling site after the TAG event shows a redder slope with respect to data acquired before the event. ID of spectra used for Nightingale area are the average: 417845-417753, for EQ3, and 826808-826809-827536, for BFF (refer to Table A1 for acquisition times and viewing and illumination conditions).

contribution of dust, highlighting true differences on the surface. The direct contribution of the dust can not be compensated in evaluating the ratio between the two observational stations used in map analysis, therefore we chose two control areas to evaluate the contribution of the dust on the final results. More information on this topic with additional tests are provided in the Appendix. Another caveat affecting the BFF data set, is higher than nominal temperatures of the OVIRS detector during the acquisition of post-TAG data set. This instrumental condition introduces additional sources of uncertainty in the spectra with increased noise and decreased sensitivity; in particular, at longer wavelengths (>2.5 μm) part of the data set was saturated and was not used in this analysis. Unfortunately, the additional detector uncertainty is not easily removed, and longer wavelength analyses have to take into account this caveat. Additional background signal and noise are partially removed by background subtraction, but no corrections are possible for the change in sensitivity. Therefore, changes in the region above 2.5 μm, in particular after 3 μm, are not possible to be quantified. Another important source of uncertainties come from different subsolar latitudes, and therefore different illumination conditions, as well as different surface temperatures between EQ3 and BFF. This can be partially removed by the photometric correction but we acknowledge a contribution from this effect in all our results. Indeed, due to different time of acquisition, both in Bennu day/night cycle and orbital position, the temperature on the surface of Nightingale were different during the acquisition of EQ3 and BFF data. As known temperature variation affect the infrared spectrum at any wavelength (De Angelis et al. 2017; Poggiali et al. 2021), in the Appendix, we present some additional analysis on this caveat.

3 RESULTS

The Nightingale site analysis post-sampling event revealed a reddening of the spectral slope and darkening of the surface in the crater area using multiple instruments including OVIRS (Lauretta et al. 2022). In Fig. 1, Nightingale site spectra ratioed with the global average both for EQ3 and BFF are shown. Using spectral ratios with the global average (obtained from the same data set) is an effective way to enhance possible differences, as performed for exogenous material discovery in DellaGiustina et al. (2021). Some differences between Nightingale spectra from EQ3 and BFF were already visible before the ratioing procedure (Appendix Fig. A1). The ratios of the sampling site spectra show that after the TAG maneuver the site become redder, moreover, we observed that both the spectra show some residual absorption near 2.7 μm linked with a deeper hydration band in the site. Spectral differences between the average surface of Bennu and the sampling site were evaluated both within the EQ3 and the BFF data sets by comparing the spectra from Nightingale with those far from the sampling site. Fig. 2, top panel, shows the continuum removed reflectance spectra between the Nightingale crater (spectrum and region number 1 in red) and nearby areas chosen at increasing distance from the sampling site (respectively spectrum and region number 2 in yellow, number 3 in green and number 4 in blue). Since no visible differences appear from the continuum-removed spectra, we decided to additionally study the ratio with the global average spectrum. In Fig. 2, bottom panel, we observed that the continuum removed ratioed spectra of sites 2, 3, and 4 (respectively yellow, green, and blue) are almost flat or show only continuum variation, whereas those of site 1 (red), centered on the Nightingale site, exhibit a subtle but clear absorption feature at 2.7 μm indicating that the hydrated phyllosilicate feature is slightly stronger in the Nightingale site. However, the changes in band depth between before and after the TAG event (respectively EQ3 in right-hand panel and BFF in left-hand panel) are not visible in the spectra over instrumental noise. A feature appears at longer wavelengths near 3.3–3.4 μm in the BFF data that is generally associated with organic/carbonate material. This feature disappears when an average of Nightingale area is used instead of a single spectra (see Fig. A3), in fact due to higher temperature of the detector, this result needs to be investigated more in detail. The imperfect linearity of the ratioed spectra in the BFF data is most likely an artefact due to the presence of shadows during the OVIRS spectrum acquisition.

Furthermore, we analysed variation maps of several spectral parameters computed from the hydrated phyllosilicate absorption band. To evaluate possible instrumental effects in this work, in addition to the Nightingale region, we analysed two other areas located far from the sampling site but similar in terms of viewing geometry during acquisition to the primary site. Control Area A was chosen in the Northern hemisphere of Bennu, at a similar latitude to Nightingale but on the opposite side of the asteroid; control Area B was chosen at approximately the same longitude as Nightingale but in the Southern hemisphere of the asteroid (Fig. 3). For the three named areas, four spectral parameters calculated from the phyllosilicate absorption band were evaluated (band minimum position and band depth in Fig. 4, band area and NOPL in Fig. A5). In Fig. 4, the maps for band minimum position and band depth obtained ratioing EQ3 and BFF maps are shown, illustrating variation between pre- and post-TAG. Ratios between spectra acquired in different observational stations are done after the photometrical correction to eliminate possible geometrical effects, even if contribution from shadows and different illumination angles derived from different subsolar latitude can remain. As visible in Fig. 4 top panels, we found no differences either in Nightingale or in control areas for the position of the band minimum considering the error on minimum position. As visible in the band depth BFF/EQ3 ratio map for each analysed spot (Fig. 4, bottom panels), a variation of about 19 per cent is visible in some part of Nightingale site. We must note, however, that this variation is also present with a decreased intensity of 10–12 per cent at the control

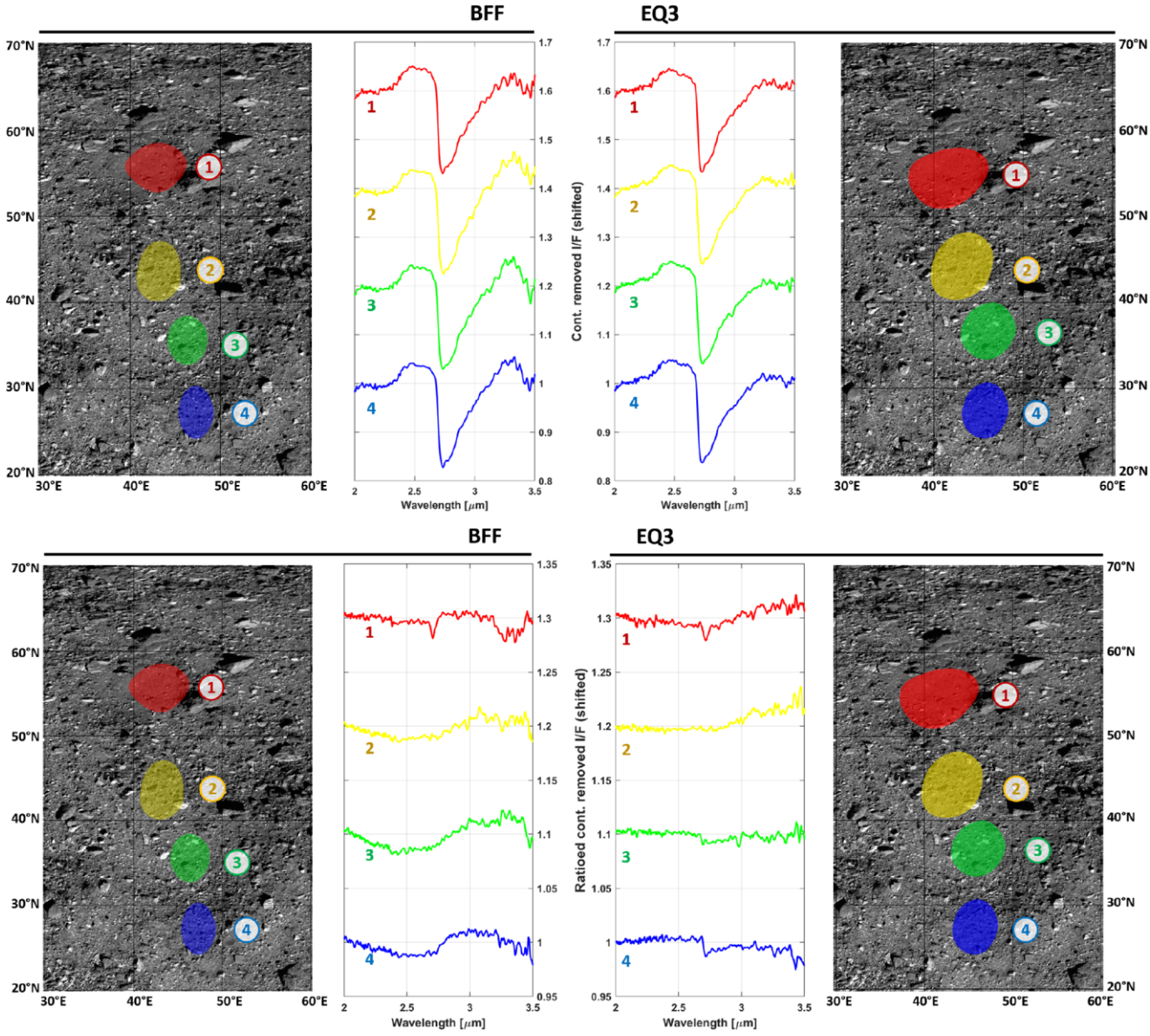

Figure 2. OVIRS spectra acquired over the Nightingale region according to the coloured footprint shown in corresponding side panel for EQ3, right-hand panels, and BFF, left-hand panels. From blue to red, spectra are closer to the sampling site corresponding to the last red footprint. The top panels show the spectra continuum removed from 2 to 3.5 μm. Ratios of the respective global average are showed in the bottom panels. The spectra are vertically shifted for clarity. Original spectra are showed in the Appendix Fig. A2. ID of spectra used for EQ3 are: 417845 (n.1), 417750 (n.2), 417591 (n.3), and 417594 (n.4). ID of spectra used for BFF are: 826808 (n.1), 827541 (n.2), 826800 (n.3), and 826797 (n.4). Reader can refer to Table A1 for acquisition time and geometry condition. This kind of analysis was used to analysed Ryugu sampling crater (Kitazato et al. 2021).

sites (located away from Nightingale, thus not disturbed by the TAG event). These differences between Nightingale and control areas are discussed, together with previous results, in the next section.

4 DISCUSSION

Nightingale was selected as primary sampling site on the basis of safety, sampleability, and scientific value criteria. Image analysis before TAG identified material with grain size < 2 cm (sampleable material) and OVIRS spectra collected from the area showed a redder slope compared with the nearby regions and in general with Bennu's global average surface. Several factors can induce and affect a spectral slope reddening in the near-infrared region (Barucci et al. 2020), the most important are: presence of small grain size particles (Cloutis et al. 2018) and space weathering (Lantz et al. 2017). In the case of space weathering, laboratory studies showed that on CM and CI carbonaceous chondrites, proposed as good spectroscopic analogs for Bennu (Hamilton et al. 2019), ion irradiation induces a blueing of the infrared spectrum over time (Lantz et al. 2017). Therefore, the original red spectrum of Nightingale could have been related to the abundance of fine material, or to the presence of less altered material due to the relative young age of the crater with respect to the average surface of Bennu, or a combination of both.

As consequences of the TAG maneuver to collect surface sample, a large debris plume was mobilized from the surface of Nightingale (Lauretta et al. 2022) confirming the presence of abundant fine

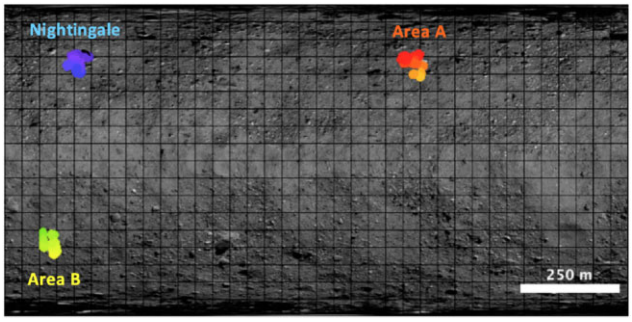

Figure 3. Location and OVIRS footprint coverage for the Nightingale site and control areas A and B analysed in this work superimposed on to Bennu's global basemap (Bennett et al. 2021).

grain material in the crater. This plume, likely formed by material either from the upper surface and excavated from the subsurface, redeposited on to the Nightingale area where it was observed during BFF almost 5 month later. The mobilization and re-deposition of fine grain material can be responsible for the reddening of the slope in the Nightingale region after TAG (Fig. 1). Of course, this does not exclude the possibility that more pristine material has been exposed by sampling, showing a spectrum less altered by space weathering. Additional analysis shows a decreased convexity of the spectrum of Nightingale after TAG event in the region 0.5–2.5 μm (Appendix Fig. A6). This result coupled with reddening of VIS-NIR spectral slope is predicted by laboratory experiment as results of space weathering processes (Lantz, Binzel & DeMeo 2018). This evidence points towards an exposure of less altered material in Nightingale area.

Regarding the content of OH and water in surface composition, although from the analysis of the individual spectra in the Nightingale region shown in Fig. 2 it is not possible to determine whether the hydration band has undergone any significant changes taking into account the caveats and the resulting estimated uncertainties of 5 per cent (see Appendix). However, from Praet et al. (2021a) the uncertainty on the band depth evaluation is about 1 per cent on EQ3 data set resulting in the overall H content variation of 5 per cent through out Bennu surface. These differences in uncertainties between the two data sets make difficult a quantitative evaluation of the absolute variation in H content. Differences not clearly visible in the band depth of single spectra for the Nightingale area become more evident once we evaluate the map for the parameters. Some spots nearby the TAG contact point showed an increased in band depth after the sampling (Fig. 4, bottom right-hamd panel). Variations appear stronger on the northern part of Nightingale crater and could be related to an asymmetrical disturbance of the area due to the combination of the TAGSAM gas mechanism and thruster firing during the back-away burn (Lauretta et al. 2022). Moreover, some variation in band depth appears also in the control areas, though with a lower intensity than seen at Nightingale. These diffuse surface variations in areas spatially distant from the sampling point are because during the BFF data acquisition, the primary mirror was contaminated with some dust as a result of the TAG maneuver. In addition, higher than normal temperature of the detector, differences in illumination conditions and in surface

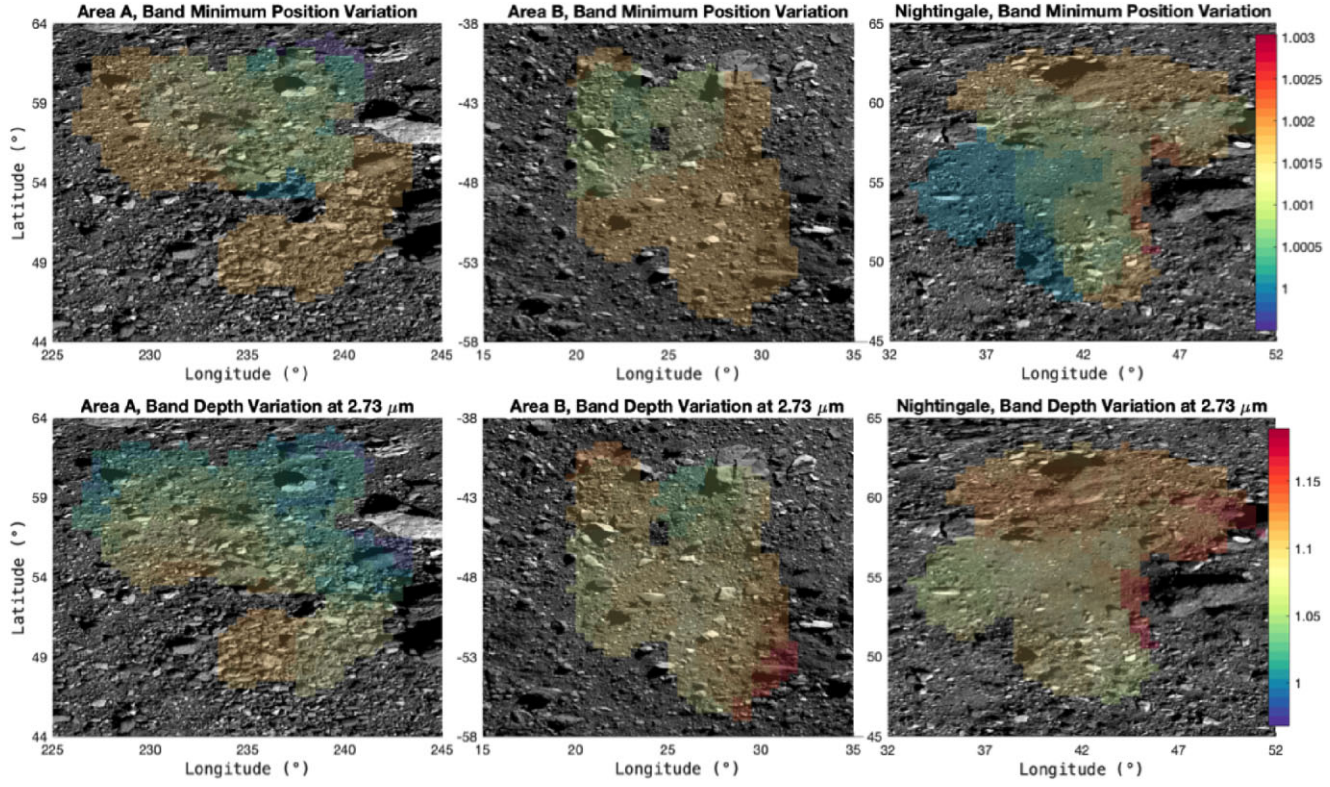

Figure 4. Maps for the hydrated phyllosilicate absorption band minimum position (top panels) and band depth (bottom panels) for Nightingale and two control regions (A and B) obtained by dividing the evaluated maps for these two parameters using data from the EQ3 and BFF observational stations. While no differences are visible in the position of the minimum, within the measurement error, the band depth shows some variation spread over all three analysed areas (the position of which can be seen in Fig. 3).

temperature caused decreased long wavelength reliability inducing few per cent uncertainty, as a result, this makes quantitatively estimations of variation percentage at Nightingale very difficult. Moreover, OH implantation could be responsible for variations across the surface as observed in other planetary bodies (McGraw et al. 2019; Tang et al. 2021). However, the greater intensity of variation on Nightingale may be indicative of real surface variation over the noise and instrumental effects, although, given the observational caveats discussed before, it becomes difficult to evaluate the real magnitude of these differences. Similar results were obtained by evaluating the ratio maps for band area and NOPL (Fig. A5) confirming that Nightingale is always characterized by some differences and the area, north of the sampling point, is the most affected by band parameter changes.

5 CONCLUSIONS

On 2020 October 20th, the OSIRIS-REx spacecraft successfully achieved the collection of a sample from asteroid Bennu's surface. The TAG maneuver on the primary sample site Nightingale mobilized material from the surface creating a 9-m crater in the centre of the sampling area. We analysed the OVIRS infrared data before and after the TAG event to evaluate possible changes in the 2.7-μm region hydration feature. Taking in account all the caveats on the data after TAG event as indicated by Lauretta et al. (2022) and described before, from spectroscopic analyses of the Nightingale area, along with two control areas on the asteroid, several results emerge:

(i) The infrared spectrum in the area of Nightingale became redder with respect to pre-TAG observations. Indicative of the exposure of finer or less space weather altered material in the crater, this result confirms previous observation (Lauretta et al. 2022). Reddening of fresh exposed material and decreased spectrum convexity is in agreement with laboratory results by Lantz et al. (2018).

(ii) The position of the 2.7-μm region absorption band minimum does not appear to vary at any of the three locations analysed, within the experimental error, suggesting no significant changes to the nature of the phyllosilicate main cation and/or no significant space weathering effect, as seen by Kitazato et al. (2021) in the case of Ryugu's surface.

(iii) Analysis of the hydrated band depth in Nightingale area and two control areas located in different region of Bennu shows some diffuse changes all over the surface due to different observational condition, detector temperature, surface temperature, and presence of dust on OVIRS optics. However, changes in Nightingale area are characterized by a slightly higher intensity that could be linked to differences in the mobilized material. The same behaviour is observed for other band parameters (band area and NOPL).

(iv) Following the caveat already discussed due to dust contamination, higher detector temperature and difference in observational geometry, the presence of the 3.3-3.4 μm band in the spectrum of Nightingale after TAG can not be firmly associated with a higher abundance of organic/carbonate material in the subsurface of Nightingale.

Analysis of infrared spectra is pivotal to understanding the nature of Bennu's surface material. Generally, variations in infrared features are caused by changes in material composition and/or its degree of alteration and their study can provide knowledge on the asteroid's evolution. The absence of strong differences in the hydration band (both for peak position and band depth) in the Nightingale area could be an effect of the re-deposition of material excavated from the subsurface mixed with the material of the top surface as a consequence of the sampling maneuver. This process could mix together new and old material reducing the magnitude of spectral variation. On the other hand, if Nightingale crater was recently formed, we might not expect strong variation in the band depth taking into account that in the space weathering processes some can reduce (e.g. impact-induced heating can cause dehydration, Nakamura 2006) and other can increase the surface hydration (solar wind implantation, Li & Milliken 2017; Tucker et al. 2019). The mobilization of fine grain dust could be also responsible for the observed spectral reddening. Therefore, if this last hypothesis is confirmed, and Nightingale subsurface material is not strongly different from the surface material, the sample collected by OSIRIS-REx, now en route back to Earth, could represent some of the most pristine components of a carbonaceous asteroid.

Samples collected by OSIRIS-REx spacecraft are now on route back to Earth with expected arrival in 2023 September. The possibility of deep and accurate micro-scale analysis on the samples will be a unique opportunity to link the surface appearance and the change observed in Nightingale with the chemical and physical properties of the material. Observing space weathering effects on Bennu grains compatible with laboratory results will help us to understand the stratigraphy of Bennu in relation with abundance of volatile material and will improve our capability to interpret spectroscopic changes, similar to the results obtained by the Hayabusa 2 team with grains from the surface of asteroid Ryugu (Pilorget et al. 2021). Moreover, from our analysis, it emerges clearly that accurately assessing the change in performance of infrared instruments as a result of dust contamination during sample collection maneuvers is pivotal for future sample return missions. This work will help in future post-TAG OVIRS calibration and the observation that OSIRIS-APEX will perform in the extended mission to asteroid (99942) Apophis in 2029 (DellaGiustina et al. 2022).

ACKNOWLEDGEMENTS

We are grateful to the entire OSIRIS-REx Team for making the encounter with Bennu possible. This material is based upon work supported by NASA under Contract NNM10AA11C issued through the New Frontiers Program. LESIA-Observatoire de Paris authors thank the French Space Agency CNES for financial support.

DATA AVAILABILITY

OVIRS spectra (Reuter et al. 2018) for EQ3 and BFF are available via the Planetary Data System (Reuters et al. 2019).

REFERENCES

Barnouin O. S. et al., 2019, Nat. Geosci., 12, 247
Barucci M. A. et al., 2020, A&A, 637, L4
Bennett C. A. et al., 2021, Icarus, 357, 113690
Bierhaus E. B. et al., 2018, Space Sci. Rev., 214, 107
Cloutis E. A. et al., 2018, Icarus, 305, 203
De Angelis S. et al., 2017, Icarus, 281, 444
Dellagiustina D. N. et al., 2019, Nat. Astron., 3, 341
DellaGiustina D. N. et al., 2021, Nat. Astron., 5, 31
DellaGiustina D., Golish D. R., Guzewich S., Moreau M., Nolan M. C., Polit A. T., Simon A. A., 2022, LPI Contributions. p. 2011
Ferrone S. M. et al., 2021, Earth Space Sci., 8, e00613
Hamilton V. E. et al., 2019, Nat. Astron., 3, 332
Jawin E. R. et al., 2020, J. Geophys. Res. (Planets), 125, e06475
Kitazato K. et al., 2021, Nat. Astron., 5, 246
Lantz C., Brunetto R., Barucci M. A., Fornasier S., Baklouti D., Bourçois J., Godard M., 2017, Icarus, 285, 43
Lantz C., Binzel R. P., DeMeo F. E., 2018, Icarus, 302, 10
Lauretta D. S. et al., 2017, Space Sci. Rev., 212, 925

Lauretta D. S. et al., 2022, Science, 377, 7
Li S., Milliken R. E., 2017, Sci. Adv., 3, e1701471
McGraw L., Emery J., Thomas C., Rivkin A., Wigton N., 2019, EPSC-DPS Joint Meeting 2019. p. EPSC–DPS2019-709
Milliken R. E., Mustard J. F., 2007, Icarus, 189, 550
Nakamura T., 2006, Earth Planet. Sci. Lett., 242, 26
Pilorget C. et al., 2021, Nat. Astron., 6, 221
Poggiali G., Brucato J. R., Dotto E., Ieva S., Barucci M. A., Pajola M., 2021, Icarus, 354, 114040
Praet A. et al., 2021a, Icarus, 363, 114427
Praet A., Barucci M. A., Hasselmann P. H., Kitazato K., Iwata T., Matsuoka M., Domingue D., Clark B. E., 2021b, A&A, 649, L16
Reuter D. C. et al., 2018, Space Sci. Rev., 214, 54
Reuters D. C., Simon A. A., Lunsford A., Lauretta D. S., 2019, NASA Planetary Data System
Simon A. A. et al., 2020a, Science, 370, eabc3522
Simon A. A. et al., 2020b, A&A, 644, A148
Simon A. A., Reuter D. C., Lauretta D. S., 2021, J. Astron. Telesc. Instrum. Syst., 7, 020501
Tang H. et al., 2021, Icarus, 359, 114322
Tucker O. J., Farrell W. M., Killen R. M., Hurley D. M., 2019, J. Geophys. Res. (Planets), 124, 278
Walsh K. J. et al., 2019, Nat. Geosci., 12, 242
Zou X.-D. et al., 2021, Icarus, 358, 114183

APPENDIX A: DATA SET INFORMATION AND QUALITY ASSESSMENT

Spectra used in our work are part of the EQ3 and BFF data sets. EQ3 spectra were acquired on 2019 May 9 from about ∼5 km above the surface. The spot spatial resolution, resulting from 4 *mrad* field of view, was ∼20 m. Spacecraft was located approximately above the equator, scanning north–south at local solar time 12:30 pm. In BFF, observations were performed on 2021 April 7 from 3.7 km with ∼12 m spatial resolution. The spacecraft trajectory was similar to EQ3 with equatorial sub-spacecraft latitude and 12:30 pm local solar hour sub-spacecraft longitude. Information on observational conditions and geometry for the single spectra used in the analysis are reported in Table A1 .

OVIRS instrument transmission efficiency decreased by about 5 per cent due to dust deposited on the mirror during sample collection affecting all the measurements after TAG event (Lauretta et al. 2022). Moreover several other caveats were identified by authors in comparing the two data sets. Below, we present some consideration on the evaluation of data quality and accuracy of the analysis presented in this work. To determine if the global average is appropriate for the ratio procedure (due to the fact that it could include bad data), we evaluate an average of good data near the same position of Nightingale region (latitudes 52°–58° and longitudes 60°–200°) in both data sets. As visible in Fig. A3, top left-hand panel, comparing the global average with the selected average, no strong modification appear in the spectrum. When we use the two different averages to divide Nightingale region spectra, no strong differences appear (right-hand panel). We observe that spectra in EQ3 are likely less affected by selecting a different region due to BFF bad data, however, the residual band at 2.7 μm remain. Moreover, we observe that using an average of 3 spectra for Nightingale region instead of the single spectrum used in Fig. 2, the 3.3–3.4 μm is strongly reduced and absent using the special region average reinforcing the hypothesis that this part of the spectrum is the most affected by caveats.

Regarding subsolar latitudes and therefore different illumination and geometrical conditions, some additional influences on spectra comparison can arise. Observational geometry differences are taken out by photometrical correction (Zou et al. 2021), while the differences due to shadowing induced by different time on Bennu cannot be easily corrected. In fact, the equatorial region characterized by more boulders shows some relatively high values in the hydrated band depth ration between BFF and EQ3. However, our regions of interest are selected in relatively flat surface that should reduce influences by shadowing. Acquiring spectra at different temperature can also affect the infrared features, in particular the band depth. This effect was observed both on Bennu (Simon et al. 2020a) and in laboratory at any wavelength (De Angelis et al. 2017; Poggiali et al. 2021). Preliminary estimates of the Nightingale surface temperature was 329 K at EQ3 and 363 K at BFT, a differences of about 35 K. From Simon et al. (2020a), temperature differences in the same observational station of about 30 K induce an absolute band depth change of about 4 per cent (∼30 per cent by ratio), but this would result in decreased band depth, not an increase. Indeed, the increase at almost all locations indicates that another effect may be at play and we are observing the combined result.

Indeed, as seen in Fig. A4, nearly all latitudes show an increase in band depth, especially the hottest regions at the equator (where some spectral saturation is also observed). A likely culprit for the observed trend in Fig. A4 is a poor thermal tail removal. As described in Simon et al. (2020a), the surface thermal radiance is removed by first calculating a scaled solar radiance with a spectral slope defined by Bennu itself. That radiance is removed and the residual thermal tail is iteratively fitted to find the best-fitting blackbody temperature and emissivity. However, after the TAG event, the dust on the optics decreases the observed radiance, with an unknown but likely non-negligible effect at longer wavelengths. Thus, the dust is likely affecting this fit, as the method assumes pre-TAG instrument performance.

Table A1. Observational conditions for the individual spectra used in this work.

SCLK	UTC	Latitude	Longitude	Phase ang.	Inc. ang.	Emis. ang.
610709505	2019-05-09 21:32:27.375	36.69	46.06	7.85	38.26	33.87
610709508	2019-05-09 21:32:30.175	27.17	45.71	7.91	57.56	54.08
610709651	2019-05-09 21:34:53.075	43.65	43.00	7.82	66.07	62.08
610709653	2019-05-09 21:34:55.775	55.37	43.59	7.79	37.23	34.48
610709738	2019-05-09 21:36:20.075	55.36	41.59	7.79	38.94	33.95
671048585	2021-04-07 06:24:19.373	27.14	47.31	9.05	57.59	57.16
671048588	2021-04-07 06:24:22.173	35.81	46.31	9.13	52.00	49.88
671048595	2021-04-07 06:24:29.473	56.10	42.77	9.34	36.46	36.48
671048596	2021-04-07 06:24:30.373	57.48	42.39	9.37	44.12	44.77
671048684	2021-04-07 06:25:58.273	56.42	40.75	9.35	33.37	30.46
671048688	2021-04-07 06:26:02.873	42.88	43.15	9.21	54.89	53.58

Table A2. Observational characteristics of selected spectra analysed in spectral parameter variation mapping.

SCLK	UTC	Latitude	Longitude	Inc. ang.	Emis. ang.	Phase ang.
Nightingale						
610709415	2019-05-09 21:30:57.675	53.97	49.04	47.87	46.11	7.79
610709416	2019-05-09 21:30:58.575	57.12	49.22	43.53	41.40	7.78
610709498	2019-05-09 21:32:20.975	59.69	47.47	46.73	44.22	7.78
610709499	2019-05-09 21:32:21.875	56.92	47.22	42.43	40.35	7.79
610709500	2019-05-09 21:32:22.775	53.82	46.98	49.03	47.11	7.79
610709501	2019-05-09 21:32:23.775	49.91	46.72	53.03	50.45	7.80
610709652	2019-05-09 21:34:54.875	51.50	43.37	55.79	53.27	7.80
610709653	2019-05-09 21:34:55.775	55.37	43.60	45.63	43.23	7.79
610709654	2019-05-09 21:34:56.675	57.87	43.75	42.61	39.35	7.78
610709655	2019-05-09 21:34:57.575	60.79	43.97	48.46	45.76	7.78
610709736	2019-05-09 21:36:18.175	60.89	42.08	48.48	45.95	7.78
610709737	2019-05-09 21:36:19.175	57.68	41.78	41.79	38.96	7.79
610709738	2019-05-09 21:36:20.075	55.36	41.60	45.94	43.17	7.80
610709738	2019-05-09 21:36:20.975	51.47	41.31	57.66	54.76	7.81
610709890	2019-05-09 21:38:52.976	52.14	37.89	59.82	55.94	7.81
610709891	2019-05-09 21:38:53.976	55.87	38.11	48.26	44.38	7.80
610709892	2019-05-09 21:38:54.876	58.60	38.28	45.87	43.32	7.79
610709893	2019-05-09 21:38:55.776	61.82	38.55	47.51	44.90	7.78
610709974	2019-05-09 21:40:16.376	59.37	36.42	46.69	44.05	7.79
610709975	2019-05-09 21:40:17.276	56.49	36.16	50.33	46.56	7.80
671048313	2021-04-07 06:19:47.373	59.58	47.89	49.25	51.31	9.43
671048398	2021-04-07 06:21:12.573	60.64	45.71	49.99	51.28	9.44
671048399	2021-04-07 06:21:13.473	58.82	46.25	46.98	48.54	9.41
671048593	2021-04-07 06:24:27.673	51.19	43.89	58.89	60.00	9.30
671048594	2021-04-07 06:24:28.573	54.37	43.20	51.39	52.95	9.32
671048595	2021-04-07 06:24:29.473	56.11	42.77	42.66	43.76	9.35
671048596	2021-04-07 06:24:30.373	57.48	42.39	42.18	42.95	9.37
671048597	2021-04-07 06:24:31.273	59.21	41.89	47.87	49.36	9.40
671048598	2021-04-07 06:24:32.173	60.75	41.39	49.73	51.53	9.42
671048682	2021-04-07 06:25:56.473	59.88	39.86	49.71	51.66	9.40
671048683	2021-04-07 06:25:57.373	57.92	40.39	44.41	45.82	9.38
671048684	2021-04-07 06:25:58.273	56.43	40.76	42.13	42.67	9.35
671048685	2021-04-07 06:25:59.273	54.93	41.08	49.16	49.73	9.32
671048686	2021-04-07 06:26:00.173	52.04	41.68	59.64	60.10	9.30
671048879	2021-04-07 06:29:13.373	55.38	36.80	51.60	51.00	9.32
Area A						
610700979	2019-05-09 19:10:21.669	56.30	243.70	41.15	47.54	8.70
610701135	2019-05-09 19:12:57.369	52.43	240.13	49.61	53.66	8.62
610701136	2019-05-09 19:12:58.269	56.36	240.13	39.98	44.89	8.66
610701137	2019-05-09 19:12:59.169	58.62	240.08	39.44	44.87	8.71
610701138	2019-05-09 19:13:00.069	62.20	240.06	52.52	56.71	8.76
610701214	2019-05-09 19:14:16.169	59.72	238.31	43.96	48.48	8.71
610701215	2019-05-09 19:14:17.069	57.00	238.28	40.63	44.96	8.66
610701215	2019-05-09 19:14:17.969	53.55	238.25	49.10	51.87	8.62
610701216	2019-05-09 19:14:18.869	49.91	238.21	47.50	50.64	8.57
610701369	2019-05-09 19:16:51.869	48.38	234.73	45.55	48.43	8.52
610701370	2019-05-09 19:16:52.769	51.81	234.72	47.41	50.81	8.56
610701371	2019-05-09 19:16:53.669	55.14	234.71	46.39	50.10	8.61
610701372	2019-05-09 19:16:54.569	58.48	234.69	45.13	48.94	8.65
610701373	2019-05-09 19:16:55.469	61.99	234.68	51.33	55.11	8.70
610701449	2019-05-09 19:18:11.569	60.79	232.89	49.18	53.13	8.67
610701450	2019-05-09 19:18:12.469	57.46	232.85	44.38	47.95	8.62
610701451	2019-05-09 19:18:13.369	54.24	232.81	46.04	49.97	8.58
610701452	2019-05-09 19:18:14.269	50.76	232.77	48.46	52.01	8.53
610701607	2019-05-09 19:20:49.069	54.39	229.28	43.19	47.27	8.54
610701607	2019-05-09 19:20:49.969	57.59	229.27	44.45	48.01	8.59
671056076	2021-04-07 08:29:10.078	55.05	241.65	49.69	48.02	9.78
671056077	2021-04-07 08:29:11.978	50.26	240.71	52.23	50.44	9.83
671056078	2021-04-07 08:29:12.878	48.15	240.34	49.64	46.66	9.86
671056268	2021-04-07 08:32:22.478	49.57	236.46	52.71	48.80	9.89
671056271	2021-04-07 08:32:25.178	55.90	237.68	52.76	47.61	9.80
671056273	2021-04-07 08:32:27.078	59.17	238.47	49.13	46.34	9.75
671056273	2021-04-07 08:32:27.978	60.92	238.96	53.64	50.50	9.73
671056358	2021-04-07 08:33:52.278	59.42	236.57	52.81	49.28	9.77

Table A2 *– continued*

SCLK	UTC	Latitude	Longitude	Inc. ang.	Emis. ang.	Phase ang.
671056359	2021-04-07 08:33:53.178	57.87	236.13	50.24	46.36	9.80
671056360	2021-04-07 08:33:54.078	56.17	235.67	52.03	47.87	9.82
671056556	2021-04-07 08:37:10.078	56.07	231.49	49.76	46.70	9.87
671056556	2021-04-07 08:37:10.978	57.69	231.90	49.19	45.96	9.85
671056557	2021-04-07 08:37:11.878	59.34	232.36	52.09	48.61	9.82
671056643	2021-04-07 08:38:37.078	59.73	230.50	53.18	49.40	9.84
671056643	2021-04-07 08:38:37.978	58.17	230.02	49.72	45.82	9.86
Area B						
610710012	2019-05-09 21:40:54.876	−46.29	32.96	51.76	57.14	9.27
610710013	2019-05-09 21:40:55.776	−50.42	32.89	55.59	61.18	9.33
610710091	2019-05-09 21:42:13.576	−52.12	31.00	55.29	60.80	9.37
610710092	2019-05-09 21:42:14.576	−47.43	31.06	53.98	59.72	9.31
610710093	2019-05-09 21:42:15.476	−43.19	31.10	49.56	54.28	9.25
610710250	2019-05-09 21:44:52.076	−43.56	27.45	51.45	57.07	9.29
610710250	2019-05-09 21:44:52.976	−48.10	27.37	53.74	59.15	9.35
610710251	2019-05-09 21:44:53.876	−51.94	27.29	52.89	57.92	9.41
610710329	2019-05-09 21:46:11.776	−50.90	25.44	51.10	55.92	9.42
610710330	2019-05-09 21:46:12.676	−47.23	25.49	52.96	57.89	9.36
610710331	2019-05-09 21:46:13.576	−42.58	25.53	51.99	57.65	9.30
610710487	2019-05-09 21:48:49.276	−41.18	21.94	51.19	57.22	9.31
610710488	2019-05-09 21:48:50.176	−44.52	21.88	49.80	55.73	9.37
610710489	2019-05-09 21:48:51.176	−48.91	21.79	51.25	56.26	9.43
671049584	2021-04-07 06:40:58.674	−42.79	29.17	48.22	51.82	9.45
671049586	2021-04-07 06:41:00.574	−48.12	29.67	49.95	54.59	9.51
671049587	2021-04-07 06:41:01.474	−50.30	29.90	47.62	52.03	9.54
671049588	2021-04-07 06:41:02.374	−52.24	30.12	48.43	52.10	9.57
671049678	2021-04-07 06:42:32.174	−53.71	28.42	51.36	54.12	9.62
671049679	2021-04-07 06:42:33.074	−51.77	28.12	46.60	49.44	9.59
671049679	2021-04-07 06:42:33.974	−49.91	27.86	47.35	50.29	9.56
671049680	2021-04-07 06:42:34.874	−47.67	27.57	49.91	53.76	9.53
671049682	2021-04-07 06:42:36.674	−42.70	27.01	48.48	52.75	9.48
671049867	2021-04-07 06:45:41.774	−41.56	22.25	45.47	49.99	9.54
671049868	2021-04-07 06:45:42.674	−43.60	22.39	46.73	51.45	9.57
671049869	2021-04-07 06:45:43.574	−46.14	22.59	46.84	50.42	9.60
671049870	2021-04-07 06:45:44.474	−48.09	22.75	47.22	49.87	9.63
671049871	2021-04-07 06:45:45.374	−50.22	22.94	46.78	49.89	9.66

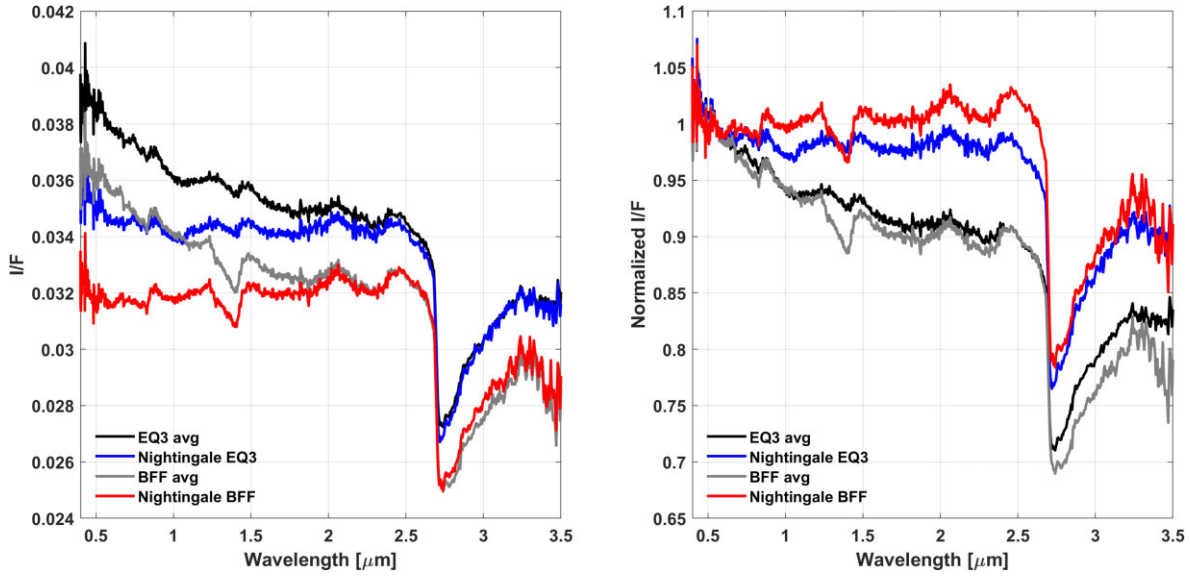

Figure A1. OVIRS spectra of Nightingale before (blue line) and after (red line) the sampling event, along with global average by data set EQ3 (black line) and BFF (grey line), respectively, acquired before and after the sampling event. Right-hand panel shows original intensities while left-hand panel shows spectra normalized at 0.55 μm. Looking at the right-hand panel, spectra in BFF show a reduction in intensity linked with dust on the OVIRS mirror (Lauretta et al. 2022), once normalized at 0.55 μm (left-hand panel) spectra in Nightingale site revealed a reddening in spectra acquired during BFF with respect to spectra acquired in EQ3. ID of spectra used for Nightingale area are the average: 417845-417753, for EQ3, and 826808-826809-827536, for BFF (refer to Table A1 for acquisition time and geometry condition).

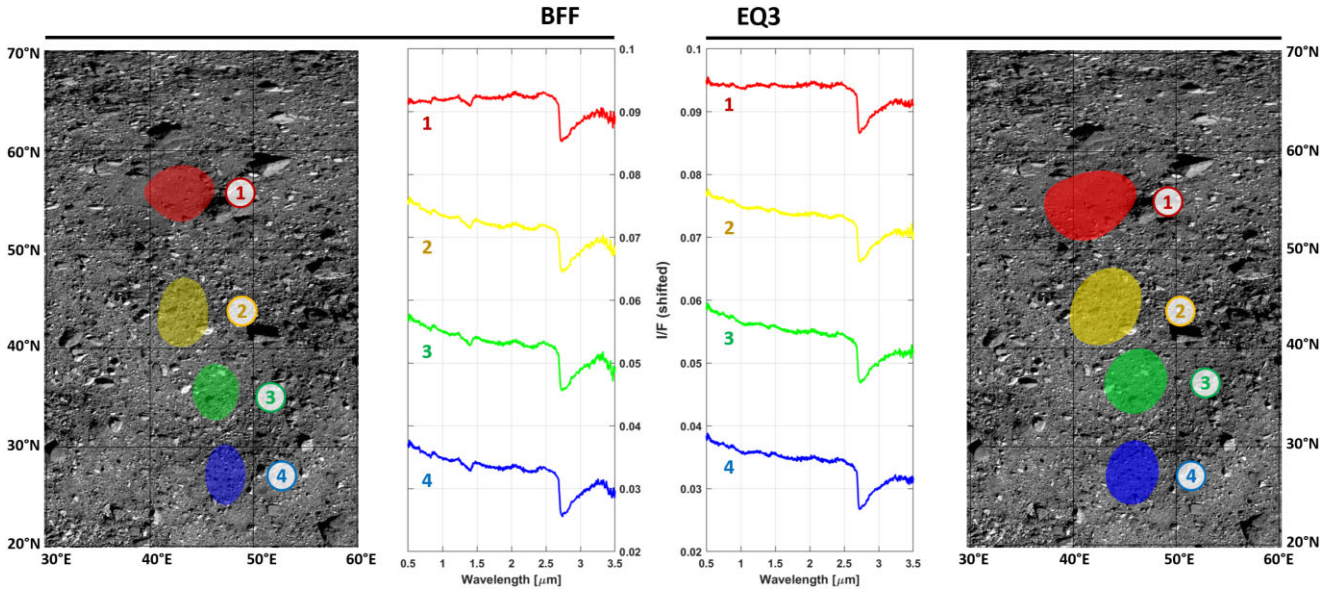

Figure A2. OVIRS spectra acquired over the Nightingale region according to the coloured footprint shown in corresponding side panel for EQ3, right-hand panels, and BFF, left-hand panels. From blue to red, spectra are closer to the sampling site corresponding to the last red footprint. ID of spectra used for EQ3 are: 417845 (n.1), 417750 (n.2), 417591 (n.3), and 417594 (n.4). ID of spectra used for BFF are: 826808 (n.1), 827541 (n.2), 826800 (n.3), and 826797 (n.4). Reader can refer to Table A1 for acquisition time and geometry condition.

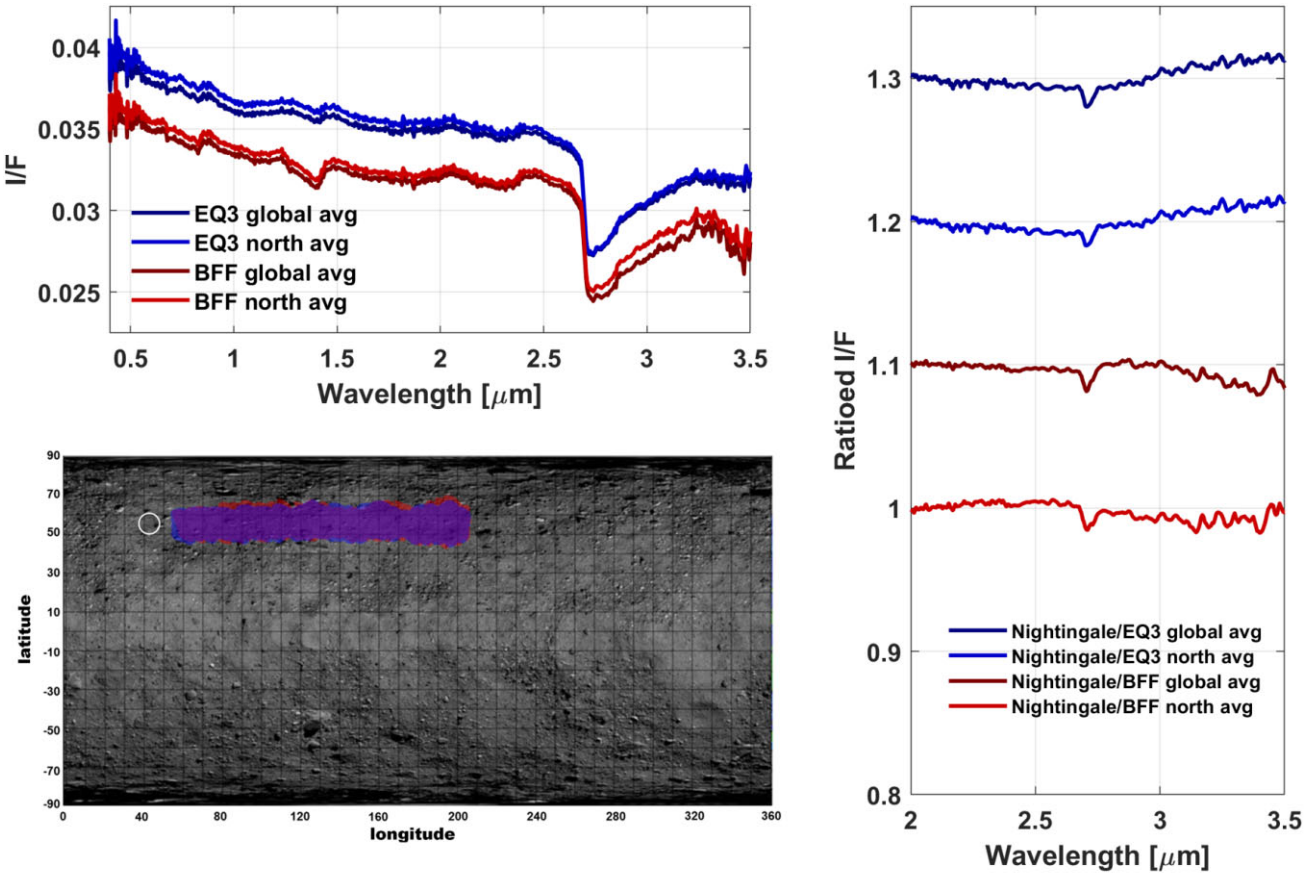

Figure A3. Evaluation of differences due to the ratio with global average and a selection of spectra from the region latitudes 52°–58°, and longitudes 60°–200° (position shown in the bottom left-hand panel) As visible in the top left-hand panel, differences between the two average in the two data set are mostly in intensity, when ratioed the area of Nightingale for the average in both data set no strong differences appear in the spectrum.

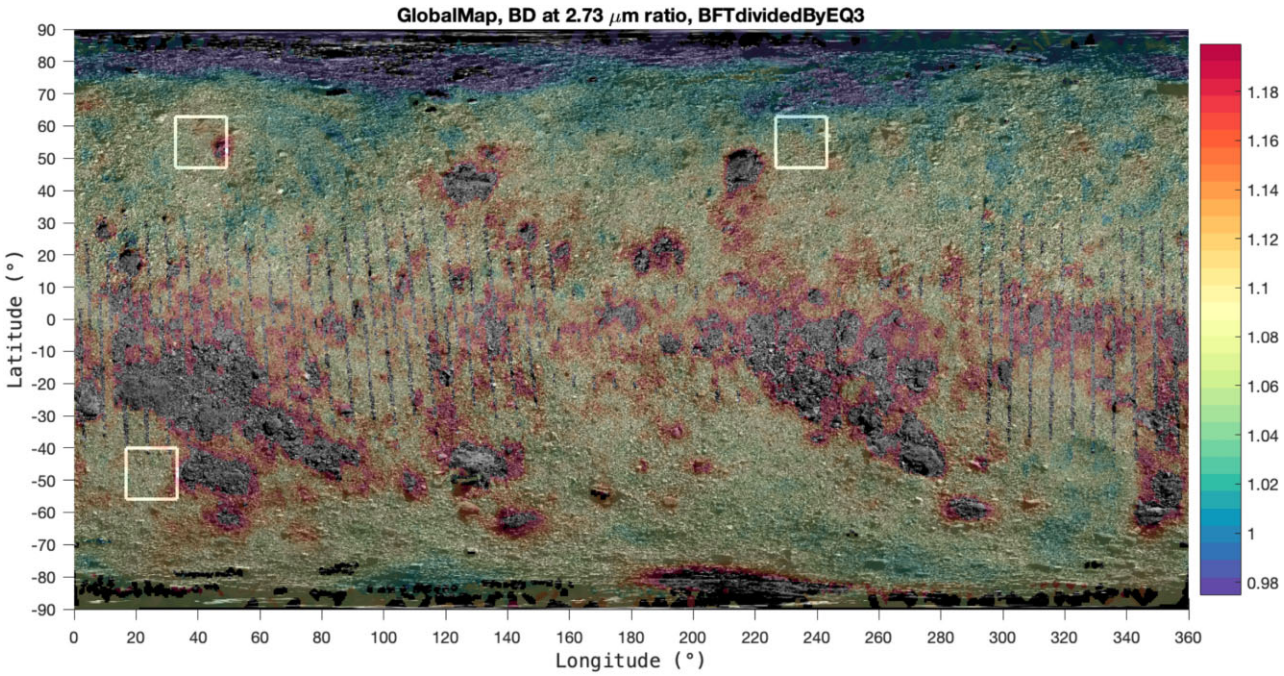

Figure A4. Global map for 2.7-μm region band depth ratio obtained by dividing the evaluated maps for this parameter using data from EQ3 and BFF observational stations.

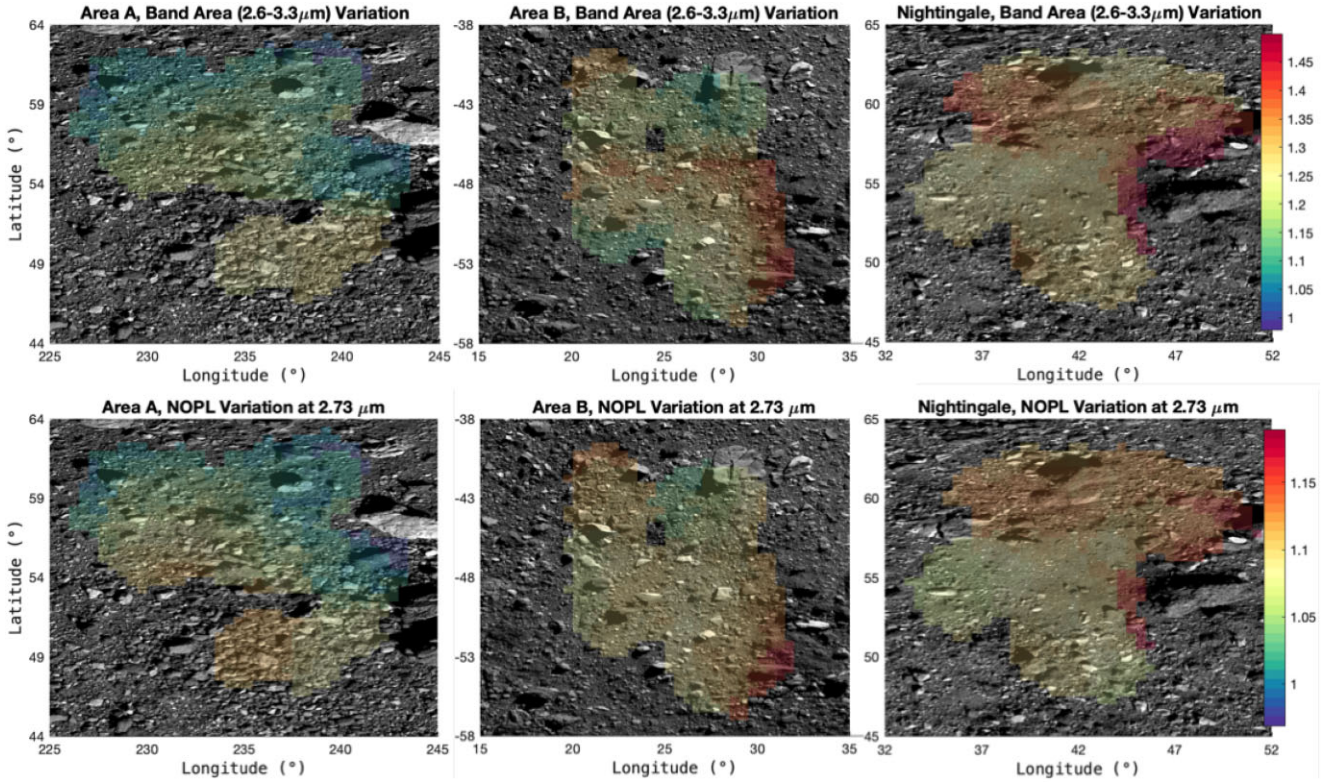

Figure A5. Ratio maps for 2.7-μm region band area (top panels) and NOPL (bottom panels) for Nightingale and two control regions obtained by dividing the evaluated maps for these two parameters using data from EQ3 and BFF observational stations. While no difference is visible in the position of the minimum, within the measurement error, the band depth shows a variation of about 5 per cent for band area and 15 per cent for NOPL spread over all three analysed areas (the position of which can be seen in Fig. 3).

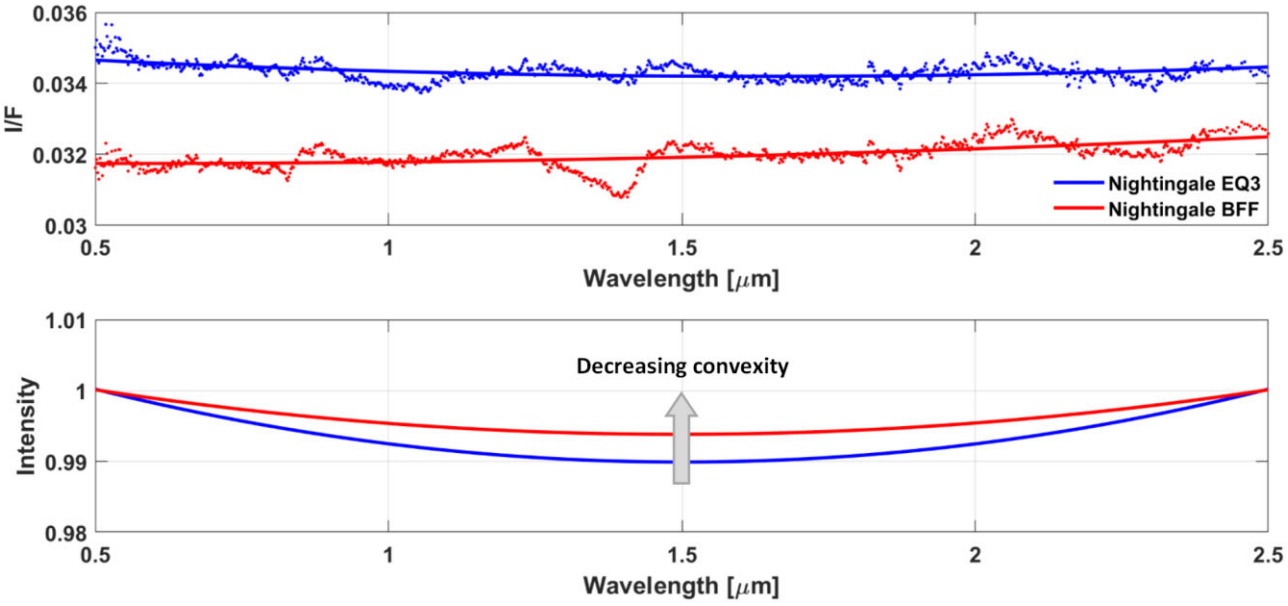

Figure A6. Top panel, averaged spectra of Nightingale site in the region 0.5−2.5 μm collected during EQ3 (blue dots) and after TAG event (red dots), polynomial fit of second degree are superimposed over spectra data with same colour legend. Bottom panel, polynomial second degree fit of Nightingale spectrum before TAG event (blue) and after (red) with continuum removed between 0.5 and 2.5 μm. The reduction in spectral convexity is in good agreement with the prevision on space weathering effect obtained by laboratory measurements (Lantz et al. 2018).

This paper has been typeset from a TEX/LATEX file prepared by the author.